

# Flexible vector-based spatial configurations in land models

Shervan Gharari<sup>1,\*</sup>, Martyn P. Clark<sup>1</sup>, Naoki Mizukami<sup>2</sup>, Wouter J. M. Knoben<sup>1</sup>, Jefferson S. Wong<sup>3</sup>, Alain Pietroniro<sup>4</sup>

1- University of Saskatchewan Coldwater Laboratory, Canmore, Alberta, Canada.

2- National Center for Atmospheric Research, Boulder, Colorado, USA.

3- Global Institute for Water Security (GIWS), Saskatoon, Saskatchewan, Canada.

4- Environment and Climate Change Canada (ECCC), Saskatoon, Saskatchewan, Canada.

\*Corresponding author Shervan Gharari, [shervan.gharari@usask.ca](mailto:shervan.gharari@usask.ca)

**Abstract.** Land models are increasingly used in terrestrial hydrology due to their process-oriented representation of water and energy fluxes. A priori specification of the grid size of the land models is typically defined based on the spatial resolution of forcing data, the modeling objectives, the available geo-spatial information, and computational resources. The variability of the inputs, soil types, vegetation covers, and forcing are masked or aggregated based on the *a priori* grid size. In this study, we propose an alternative vector-based implementation to directly configure a land model using unique combinations of land cover types, soil types, and other desired geographical features that has hydrological significance, such as elevation zone, slope, and aspect. The main contributions of this paper are to (1) implement the vector-based spatial configuration using the Variable Infiltration Capacity (VIC) model; (2) illustrate how the spatial configuration of the model affects simulations of basin-average quantities (i.e., streamflow) as well as the spatial variability of internal processes (SWE and ET); and (3) describe the work/challenges ahead to improve the spatial structure of land models. Our results show that a model configuration with a lower number of computational units, once calibrated, may have similar accuracy to model configurations with more computational units. However, the different calibrated parameter sets produce a range of, sometimes contradicting, internal states and fluxes. To better address the shortcomings of the current generation of land models, we encourage the land model community to adopt flexible spatial configurations to improve model representations of fluxes and states at the scale of interest.

## 1 Introduction

Land models have evolved considerably over the past few decades. Initially, land models (or land-surface models) were developed to provide the lower boundary conditions for atmospheric models (Manabe, 1969). Since then land models have increased in complexity, and they now include a variety of hydrological, biogeophysical, and biogeochemical processes (Pitman, 2003). Including this broad suite of terrestrial processes makes land models enables simulations of energy and water fluxes and carbon and nitrogen cycles.

Despite the recent advancements in process representation in land models, there is currently limited understanding of the appropriate spatial complexity that is justified based on the available data and the purpose of the modelling exercise (Hrachowitz and Clark, 2017). The increase of computational power, along with the existence of more accurate digital elevation models and land cover maps, encourage modelers to configure their models at the finest spatial resolution possible. Such hyper-resolution implementation of land models (Wood et al., 2011) can provide detailed simulations at spatial scales as small as 1-km<sup>2</sup> grid over large geographical domains (e.g., Maxwell et al., 2015). However, the computational expense for hyper-resolution models could potentially be reduced using more creative spatial discretization strategies (Clark et al., 2017).

It is common to adopt concepts of hydrological similarity to reduce computational costs. In this approach, spatial units are defined based on similarity in geospatial data, under the assumption that processes, and therefore parameters, are similar for areas within a spatial unit (e.g., Vivoni et al., 2004, Newman et al., 2014). Hydrological Response Units (HRUs) are perhaps the most well-known technique to group geospatial attributes in hydrological models. HRUs can be built based on various geospatial characteristics; for example, Kirkby and Weyman 1974, Knudsen and Refsgaard (1986), Flügel (1995), Winter (2001), and Savenije (2010) all have proposed to use geospatial indices to discretize a catchment into hydrological units with distinct hydrological behaviour. HRUs can be built based on soil type such as proposed by Kim and van de Giessen (2004). HRUs can also be built based on fieldwork and expert knowledge (Naef et al., 2002, Uhlenbrook 2001), although the spatial domain of such classification will be limited to the catchment of interest and the spatial extent of the field measurements. HRUs are often constructed by GIS-based overlaying of various maps of different characteristics and can have various shapes

such as for non-regular (sub-basins), grid, hexagon, or triangulated irregular network also known as TIN (Beven 2001, Marsh et al., 2012, Oliviera et al., 2006). Land models are also beginning to adopt concepts of hydrological similarity (e.g., Newman et al., 2014; Chaney et al., 2018). Traditionally land models use the tiling scheme where a grid box is subdivided into several tiles of unique land cover, each described as a percentage of the grid (Koster and Suarez, 1992). Similarly, the concept of Grouped Response Units (GRUs, Kouwen et al., 1993), assumes similar hydrological property for areas with identical soil, vegetation, and topography. The GRU concept is utilized in the MESH land modeling framework (Pietroniro et al., 2007).

A long-standing challenge is understanding the impact of grid size on model simulations (Wood et al., 1988). The effect of model grid size can have a significant impact on model simulation across scale especially if the model parameters are linked to characteristics which are averaged out across scale (Bloschl et al., 1995). Shrestha et al. (2015) have investigated the performance of Community Land Model (CLM) v4.0 coupled with ParFlow across various grid sizes. They concluded the grid size changes of more than 100 meters can significantly affect the sensible heat and latent heat fluxes as well as soil moisture. Also using CLM, Singh et al. (2015) demonstrated that topography has a substantial impact on model simulations at the hillslope scale (~100 meters), as aggregating the topographical data changes the runoff generation mechanisms. This is understandable as the CLM is based on topographical wetness index (Beven and Kirkby 1979, Niu et al., 2005). However, Melsen et al. (2016) evaluated the transferability of parameters sets across the temporal and spatial resolutions for the Variable Infiltration Capacity (VIC) model implemented in an Alpine region. They concluded that parameter sets are more transferable across various grid sizes in comparison with parameter transferability across different temporal resolutions. Haddeland et al. (2002) showed that the transpiration from the VIC model highly depends on grid resolution. It remains debatable how model parameters and performance can vary across various grid resolutions (Liang et al., 2004; Troy et al., 2008; Samaniego et al., 2017).

The representation of spatial heterogeneity is an ongoing debate in the land modelling community (Clark et al., 2015). The key issue is to define which processes are represented explicitly and which processes are parameterized. The effect of spatial scale on emergent behavior has been studied for catchment scale models – the concepts of Representative Elementary Areas (REA), or Representative Elementary Watersheds (REW), were introduced to study the effect of spatial

aggregation on system-scale emergent behavior (Wood et al., 1995, Reggiani et al., 1999). The effect of scale on model simulations is not well explored for land models. More work is needed to understand the extent to which the heterogeneity of process representations is sufficient for the purpose of a given modelling application, and the extent to which the existing data can support the model configurations (Wood et al., 2011, Beven et al., 2015) and guarantee a *fideli*us model.

In this study, we configure the Variable Infiltration Capacity (VIC) model in a flexible vector-based framework to understand how model simulations depend on the spatial configuration. The remainder of this paper is organized as follows: In Section 2, we present the concept of vector-based configuration for land models. In Section 3 we describe the study area and the data sets used in this study as well as the design of the experiments, and elaborate the Variable Infiltration Capacity model (VIC) and mizuRoute as the vector-based routing model. In Section 4 we describe the results of the experiments. Section 5 discusses the implication of spatial discretization strategies on large-scale land model applications. The paper ends in Section 6 with conclusions of this study and implications for future work.

## **2 The vector-based configuration for land models**

Land models are often applied at a regularly spaced grid. Land models are typically set up at a range of spatial configurations, ranging from grid sizes of  $0.02^\circ$  to  $2^\circ$  (approximately 2 to 200 km) and applied at sub-daily temporal resolutions for simulation of energy fluxes. A priori specification of the grid size of the land models is often derived from forcing resolutions, modeling objectives, available geo-spatial data and computational resources and is usually based on modeling convenience. Figure-1e-h illustrates the typical land model configuration – here the modeler selects a cell size, and then the soil, vegetation and forcing files are all aggregated or disaggregated to the target cell size. Original data resolution and spatial distribution of soil, land cover and forcing data are smeared while upscaled to the resolution of interest. Any change in the modeling resolution will require upscaling or downscaling of the geo-physical dataset once again.

In this study, we configure the land models using non-regular shapes. Figure-1a-d presents an example of non-regular shapes created through spatial intersections of the land covers and soil types shapes. These vector-based configuration of the geospatial data are then forced at the original meteorological forcing resolution, or its upscaled or downscaled values resulting in computational

units. Therefore, each computational unit has unique geospatial data such as soil, vegetation, slope and aspect and is forced with a unique forcing. In this configuration changing of meteorological forcing resolution do not affect the decisions needed to upscale the geo-spatial data such as soil type and land cover to the grid resolution.

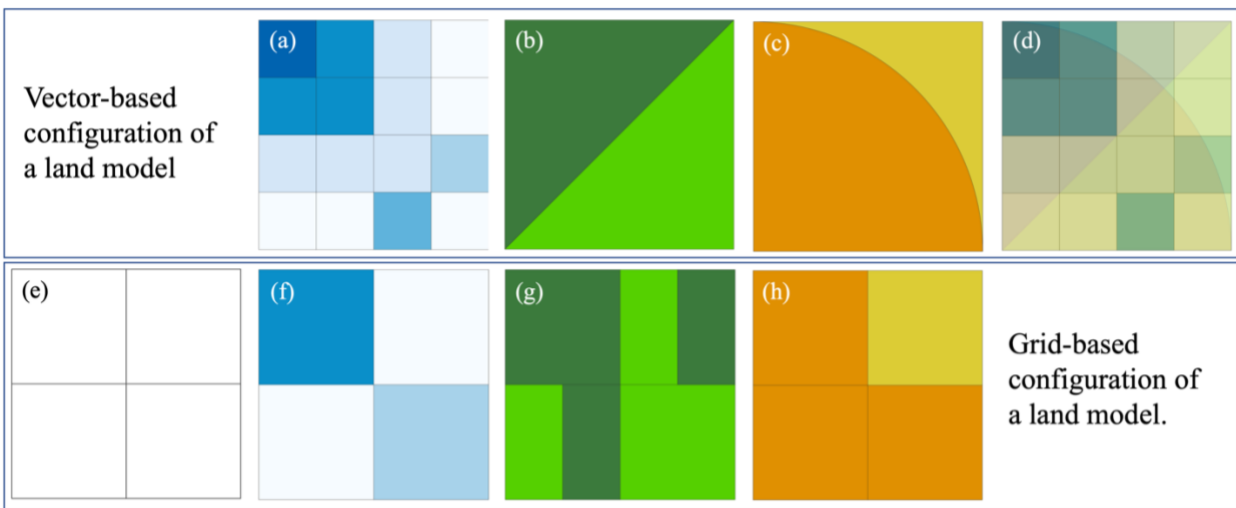


Figure-1- Top row indicates vector-based configuration of a land model; (a) meteorological forcing at its original resolution or upsampled and downsampled resolutions, (b) land covers, (c) soil types with their spatial extent, and (d) vector-based configuration with 28 computational units each with unique forcing, soil type and land cover type. The bottom row indicates typical grid-based configuration of a land model; (e) a priori resolution should be decided, (f) meteorological forcing should be upsampled or downsampled to the grid resolution, (g) land cover percentage should be calculated for each modeling grid; or a dominate landcover should be selected to represent that grid, and finally (h) soil characteristics for each modeling grid should be identified.

The benefits of vector-based configuration of land models can be summarized as follows:

**1- No need for a priori assumption on modeling grid size.** In traditional land model implementation, the modeler selects a grid resolution (which is often a regular latitude/longitude grid). The soil parameters and forcing data from any resolution must be aggregated, disaggregated, resampled or interpolated for every grid size. The land cover data often is only considered as a percentage for every grid and spatial location of the land cover is lost. However, in the vector-based setup these decisions are only based on the input and forcing data that are chosen to be used

in the modeling practice and no upscaling or downscaling to grid size is needed. Furthermore, the size of computational units can vary across modeling domain depending on the variability of the meteorological forcing and geospatial heterogeneity. For example, the spatial density of computational units can be higher in mountainous areas where temperature and precipitation gradients are larger while avoiding unnecessarily high number computational units in areas with lower gradient in meteorological forcing.

**2- Reasonable relation between available meteorological forcing and geo-spatial data resolutions and number of computational units:** computational units that are the result of available geophysical data sets forced with the original forcing data logically represent the maximum number of computational units that can be hydrologically unique. A higher number of computational units than the proposed setup will arguably provide an unnecessary computational burden due to identical forcing data and geospatial information.

**3- Direct simplification of geospatial data.** The vector-based implementation facilitates easier aggregation of computational units. It is easier to aggregate similar soil types or similar forested areas into a unified shapes with basic GIS function (dissolving for example) than this would be if all data had to be upscaled or downscaled into a different grid size.

**4- Direct specification of physical parameters and avoiding unrealistic combinations of land cover, soil and other geo-physical information.** As each computational unit has a specific type of land cover, soil type and other physical characteristics, it is straightforward to specify parameter values based on look up tables (i.e., no averaging, upscaling is needed). This is favorable because the modeler does not need to make decisions about methods used for upscaling of geophysical data at the grid level. Also, this might avoid the unrealistic combination of parameter sets that might be considered by the model at a grid scale, such as equiprobable combination of land cover on soil type which may not exist in reality which will be increasing the fidelity of the model representation of the processes (we will elaborate this further in the context of the VIC model in Discussion Section).

**5- The ability to compare and constrain the parameter values for computational units and their simulations.** The impact of land cover, soil type and elevation zone can be evaluated separately. For example, the vector-based implementation makes it easier to test if forested areas

generate less surface runoff than grasslands. This might be more challenging at the grid-based configuration in which there are combination of different land cover types at grid scale. Similarly, the vector-based implementation may simplify regularization efforts across large geographical domains. This relative constraints can be utilized to translate often patchy expert knowledge into a sophisticated land model so that the model simulation will obey the modelers and hydrologists' expectations.

**6- The possibility to incorporate additional data.** If needed, additional data, such as slope and aspect for example, can be incorporated in building the computational units, accounting for changes in shortwave radiation or lapse rates for temperature. The changes can be implemented outside of the model in the forcing files. Computational units can be built also based on variation of leaf area index (LAI) giving an additional layer of information in addition to the land cover type. The additional information can be easily ingested into the model without extra effort in contrast to changing of the model parameter files at the grid scale.

**7- Easier comparison of model simulations and in situ point-scale observation and visualization:** The vector-based implementation of land models makes it easier to compare the point measurement to model simulation as the model simulations preserve extent of geospatial features.

**8- Modular and controlled selection of models:** The vector-based implementation identifies the characteristics and spatial boundary of geospatial domains. A model might not be suitable for processes of some of the geospatial domains. Alternatively, processes of a computational unit that is beyond the capacity of one model can be replaced with an alternative model. For example, computational units that are glaciated, can be replaced with more suitable models while the spatial configuration and forcings remain identical. Consequently, the effect of features such as glaciers can be better studied as more expert models can be applied to glacier while the rest of the computational units can be simulated with a model that includes general processes.

### 3 Data and methods

#### 3.1 Study area:

Experiments are performed for the Bow River at Banff with a basin area of approximately 2210 km<sup>2</sup> located in province of Alberta, Canada. The Bow River is located in the Canadian Rockies in the headwaters of the Saskatchewan River Basin. Most of the Bow River streamflow is due to snow melt (Nivo-glacial regime). The average basin elevation is 2130 m ranging from 3420 m at the peak top to 1380 m above mean sea level at the outlet (town of Banff). The basin annual precipitation is approximately 1000 mm with range of 500 mm for the Bow Valley up to 2000 mm for the mountain peaks. The predominant land cover is conifer forest in the Bow Valley and rocks and gravels for mountain peaks above the tree line.

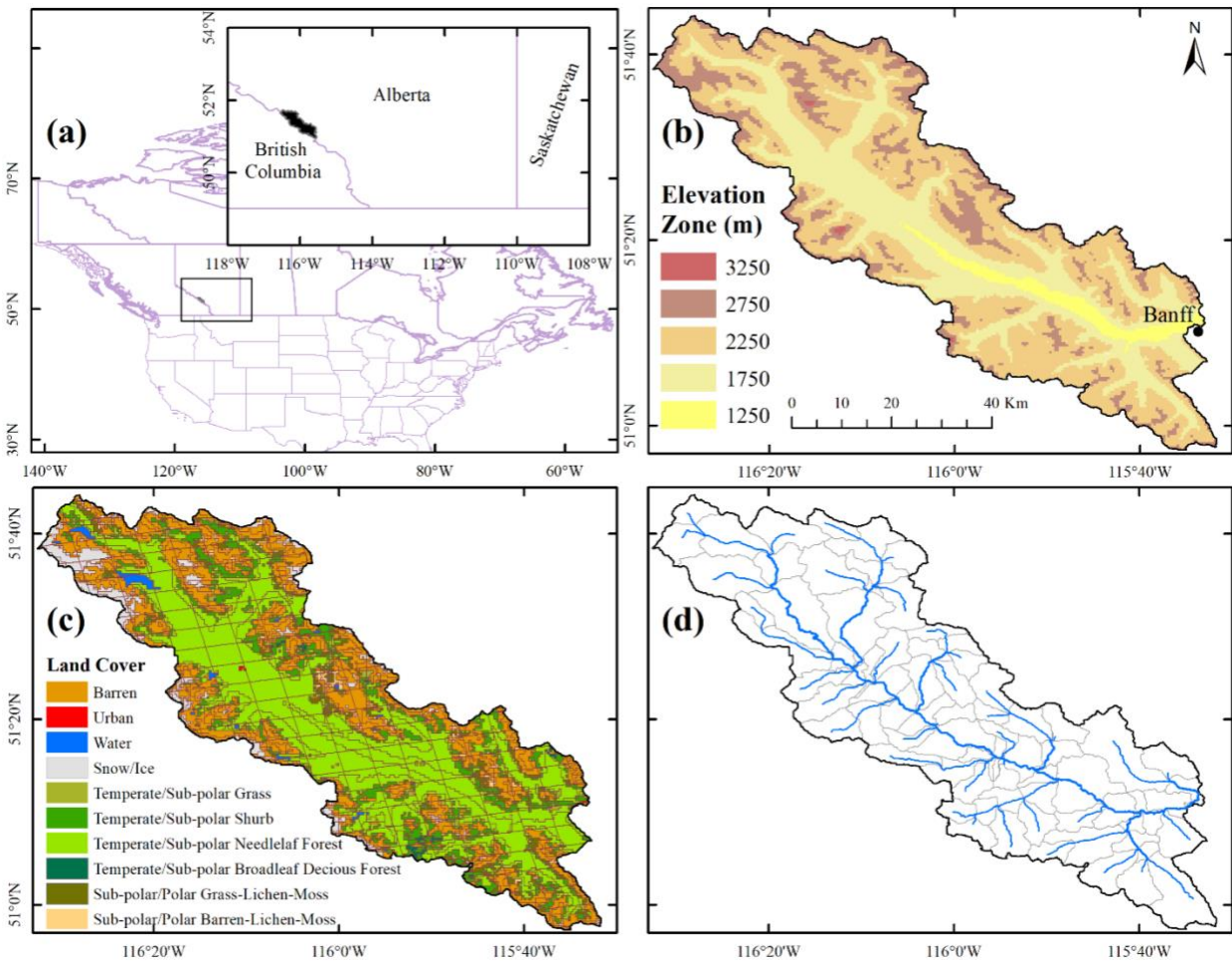




Figure – 2 (a) The location of the Bow River Basin at Banff (b) Bow River Basin elevation, (c) computational units for geospatial data of elevation zones, land cover and soil type forced at WRF original resolution at 4 km (Case-3-4km) and (d) river network topology and associated sub-basins that is used for the vector-based routing.

## 3.2 Geospatial data and meteorological forcing

### 3.2.1 Model input dataset and forcing:

The inputs and forcing we used to set up the model are as follows:

1- Land cover: We used the land cover map NALCMS-2005 v2 (North American Land Change Monitoring System, Latifovic et al., 2004) that is produced by CEC (Commission for Environmental Cooperation). NALCMS-2005 v2 includes 19 different classes. The land cover map is used to set up the vegetation file and vegetation library (look up table) for the VIC model (Nijssen et al., 2001).

2- Soil texture: We used the Harmonized World Soil Data, HWSD (Fischer et al., 2008). For each polygon of the world harmonized soil we use the highest proportion of soil type. The HWSD provide the information for two soil layers, in this study we base our analyses on the lower soil layer reported in HWSD to define the soil characteristics needed for the VIC soil file.

3- Digital Elevation Model: in this study we make use of existing hydrologically conditioned digital elevation models (DEM) to (1) derive the river network topology for the vector-based routing, mizuRoute and (2) to derive the slope, aspect and elevation zones which are used to estimate the forcing variables. For the first purpose we use hydrologically conditioned DEM of HydroSHED (Lehner et al., 2006) with resolution of 3 arc-second, approximately 90 meters; for the second purpose we use HydroSHED 15 arc-second DEM (approximately 500 meters).

4- Meteorological forcing: we used the weather research and forecasting (WRF) model simulation for continental United States with the temporal resolution of 1 hour and spatial resolution of 4 km (Rasmussen and Liu, 2017). For upscaling the WRF input forcing, we use the CANDEX package (DOI: 10.5281/zenodo.2628351) to map the 7 forcing variables to various

resolutions ( $1/16^\circ$ ,  $1/8^\circ$ ,  $1/4^\circ$ ,  $1/2^\circ$ ,  $1^\circ$  and  $2^\circ$  from the original resolution of 4 km). We used the required variables from the WRF data set namely, total precipitation, temperature, short and long wave radiation at the ground surface, V, U components of wind speed and water vapor mixing ratio.

The shortwave radiation is rescaled based on the slope and aspect of the respective computational unit (refer to Appendix-A for more details). In this study we differentiated four aspects and five slope classes. The temperature at 2 meters are adjusted using the environmental lapse rate of  $-6.5^\circ\text{C}$  for 1000 meters increase in elevation. The assumed lapse rate aligns with earlier findings from the region of study (Pigeon and Jiskoot, 2008).

### 3.2.2 Observed data for model calibration

The daily streamflow is extracted from the HYDAT (WSC, Water Survey Canada) for Bow at Banff with gauges ID of 05BB001. This data is used for parameter calibration/identification of the VIC parameters.

## 3.3 Land model and routing scheme:

### 3.3.1 The Variable Infiltration Capacity (VIC) model:

The VIC model was developed as a simple land surface/hydrological model (Liang et al. 1994) that has received applications worldwide (Melsen et al., 2016). In this study we use classic VIC version 5. The VIC model combines sub-grid probability distributions to simulate surface hydrology such as variable infiltration capacity formulation (Zhao, 1982). The VIC model uses three soil layers to represent the subsurface. While each soil layer can have various physical soil parameters (e.g., saturated hydraulic conductivity, bulk density), each layer is assumed to be uniform across the entire grid regardless of the vegetation type variability in that grid. The VIC model assumes a tile vegetation implementation within each grid similar to the mosaic approach of Koster and Suarez (1992) with bio-physical formulations for transpiration (Jarvis et al., 1976). To account for spatial variability in vegetation, the VIC model allows for root depths to be adjusted for every vegetation type. The vegetation parameters (e.g., stomatal resistance, LAI, albedo) are often identical for each land cover across the modeling domain. The VIC model can account for different elevation zones to account for temperature lapse rate given elevation difference in a grid cell, and also for the distribution of precipitation over the identified elevation zones.

In the experiments for this study, we calibrate a subset of VIC parameters namely  $b_{inf}$ ,  $E_{exp}$ ,  $K_{sat}$ ,  $d_{2,forested}$ ,  $d_{2,non-forested}$ ,  $K_{slow}$ , and  $S_{roughness}$  (names are mentioned in Table-1). Following the concept of GRU, Kouwen et al., 1993, we assume the computational units with similar geophysical characteristics (soil and land cover) possess similar parameter values. We make sure that the  $d_{2,forested}$  is larger than the  $d_{2,non-forested}$  as the root depth are deeper for forested regions (constraining relative parameters). For the sake of simplicity, we limit the root zone to the upper soil layers and replace the 5-parameter VIC baseflow<sub>1</sub> with a linear reservoir (refer to Gharari et al., 2019 for further explanation). We also assume that the two top soil layers possess homogeneous soil characteristics.

### 3.3.2 mizuRoute, a vector-based routing scheme

In this study, we make use of the vector-based routing model mizuRoute (Mizukami et al., 2016). Vector-based routing models can be configured for different computational units than the land model uses (e.g., configuring routing models using sub-basins derived from existing hydrologically conditioned DEMs such as HydroSHEDS, Lehner et al., 2006, or MERIT Hydro, Yamazaki et al., 2019). This removes the dependency of the routing on the grid size or computational unit configurations and eliminates the decisions that are often made to represent routing-related parameters at grid scale. Therefore, we can ensure that two model configurations with different geospatial configurations are routed using the same routing configuration. The intersection between the computational units in the land model and the sub-basins in the routing model defines the contribution of each computational units from the land model to each river segment.

The Impulse Response Function (IRF) routing method (Mizukami et al., 2016) is used for this study. IRF, which is derived based on diffusive wave equation, includes two parameters – wave velocity and diffusivity. The diffusive wave parameters are set to 1 m/s and 1000 m<sup>2</sup>/s respectively and remain identical for all the river segments. The river network topology, assuming approximately 25 km<sup>2</sup> starting threshold for the sub-basin size, is based on a 92-segment river network depicted in Figure-3d.

<sup>1</sup> The VIC baseflow parameters are:  $D_{smax}$ , maximum rate of baseflow;  $D_s$ , fraction of  $D_{smax}$  where non-linear baseflow begins;  $W_s$ , fraction of maximum soil moisture where non-linear baseflow occurs;  $c$ , exponent used for the non-linear part of the baseflow; and depth of the baseflow layer  $d_3$ .

284 Table-1 the VIC model parameters that are subjected to perturbation for model calibration for the  
 285 designed experiments.

Parameter symbol	Parameter name	Minimum value	Maximum value	Unit	Explanation
$b_{inf}$	Variable infiltration parameter	0.01	0.50	[-]	
$E_{exp}$	The slope of water retention curve	3.00	12.00	[-]	
$K_{sat}$	Saturated hydraulic conductivity	5.00	1000.00	[mm/day]	
$d_1$	The depth of topsoil layer	0.2	0.2	[m]	Fixed at 20 cm for both forested and non-forested computational units
$d_{2,forested}$	The depth of the second soil layer for forest computational units	0.2	2	[m]	
$d_{2,non-forested}$	The depth of the second soil layer for non-forested computational units	0.2	$d_{2,forested}$	[m]	The maximum is bounded by the $d_{2,forested}$
$D_{root}$	The distribution of root in the two soil layers	0.5	0.5	[-]	Fixed at 50% for the top and lower soil layers.
$K_{slow}$	Slow reservoir coefficient	0.001	0.9	[1/day]	
$S_{roughness}$	Snow roughness	0.5	3	[mm]	

286

### 287 3.4 Experimental design:

288 In this study, we configure the VIC model in a flexible vector-based framework to understand how  
 289 model simulations depend on the spatial configuration. We consider four different methods to  
 290 discretize the landscape for seven different spatial forcing grids (see Table 2). The landscape  
 291 discretization methods include (1) simplified land cover and soils; (2) full detail for land cover and  
 292 soils; (3) full detail for land cover and soils, including elevation zones; and (4) full detail for land  
 293 cover and soils, including elevation zones and slope and aspect. The different spatial forcing  
 294 resolutions are 4-km, 0.0625°, 0.125°, 0.25°, 0.5°, 1°, and 2°. This design enables us to separate

discretization of the landscape based on geo-spatial data from the spatial resolution of the forcing data.

Table – 2- The numbers of computational units for the Bow River at Banff, given different spatial discretization of land cover, soil type, elevation zones and slope and aspects forced with various forcing resolutions.

	Forcing resolution	<b>Case 4</b> 4 aspect groups; 5 slope groups; 19 classes of land cover; 500 meter elevation zones;	<b>Case 3</b> no aspect groups; no slope groups; 19 classes of land cover; 500 meter elevation zones;	<b>Case 2</b> no aspect groups; no slope groups; 19 classes of land cover; no elevation zones;	<b>Case 1</b> no aspect groups; no slope groups, 3 classes of land cover, one dominant soil type no elevation zones;
Number of unique combination of geo-spatial data (soil, land cover, elevation zones, slopes and	--	<b>582</b>	<b>65</b>	<b>56</b>	<b>3</b>
Number of Computational units	4 km	6631	1508	941	479
	0.0625° [~6.25 km]	5224	1098	663	290
	0.125° [~12.50 km]	3079	515	283	94
	0.25° [~25.00 km]	2013	306	154	39
	0.5° [~50.00 km]	1332	184	93	21
	1.0° [~100.00 km]	917	116	56	12
	2.0° [~200.00 km]	767	89	42	6

#### 3.4.1 Experiment-1: How does the spatial configuration affect model performance?

As the first experiment, we focus on how well the various configurations simulate observed streamflow for Bow River at Banff. We calibrate the parameters for the different configurations in Table 2. Model calibration is accomplished using the Genetic Algorithm implemented in the OSTRCIH framework (Mattot, 2005; Yoon and Shoemaker, 2001), maximizing the Nash-Sutcliffe Efficiency ( $E_{NS}$ , Nash and Sutcliffe 1970) using a total budget of 1000 model evaluations given the available resources limited by the most computationally expensive model (Case-4-4km).

#### 3.4.2 Experiment-2: How well do calibrated parameter sets transfer across different model configurations?

As the second experiment, we focus on how various configurations can reproduce the result from the configuration with highest computational units for a given parameter set. In other words, this experiment evaluates accuracy-efficiency tradeoffs – i.e., the extent to which spatial simplifications affect model performance under the assumption that similar computational units possess identical parameters across various configurations. This is important as it enables modelers to understand accuracy-efficiency tradeoffs, given the available data and the purpose of the modelling application. This experiment is based on perfect model experiments using the model with the highest computational unit as synthetic case (Case-4-4km). Synthetic streamflow for every river segment is generated using a calibrated parameter set for Case-4-4km. The models with lower number of computational units are then simulated using the exact same parameter set used for generating the synthetic streamflow. The differences in streamflow simulation, quantified using  $E_{NS}$ , provide an understanding of how the simulations deteriorate when the spatial and forcing heterogeneities are masked or upscaled. This also will bring an understanding on how sensitive the changes are along the river network and at the gauge location at which the models are calibrated against the observed streamflow data. Similarly, we compare the spatial patterns of snow water equivalent for the different spatial configurations.

## 4 Results

### 4.1 Experiment-1

The various model configurations are compared with respect to the Nash-Sutcliffe performance metric ( $E_{NS}$ ). Results show that all the models, including the ones that are configured with coarser resolution forcings, can simulate streamflow with  $E_{NS}$  as high as 0.70 (Table-3). It is noteworthy to mention that the configuration of Case-4-1° has higher  $E_{NS}$  value compared to the cases with highest computational units, Case-4-4km for example. This might be due to various reasons including: (1) compensation of forcing aggregation on possible forcing bias at finer resolution; (2) compensation of forcing aggregation on model states and fluxes and possible adjustment for model structural inadequacy and hence directing the optimization algorithm to different possible solutions across configurations.

Table-3 – The highest calibrated Nash-Sutcliffe performance metric ( $E_{NS}$ ) for the different model configurations. Details on the geospatial cases are provided in Table 2.

Forcing resolution	<b>Case 4</b> 4 aspect groups; 5 slope groups; 19 classes of land cover; 500-meter elevation zones;	<b>Case 3</b> no aspect groups; no slope groups; 19 classes of land cover; 500-meter elevation zones;	<b>Case 2</b> no aspect groups; no slope groups; 19 classes of land cover; no elevation zones;	<b>Case 1</b> no aspect groups; no slope groups; 3 classes of land cover, one dominant soil type no elevation zones;
4 km	0.80	0.81	0.78	0.75
0.0625° [~6.25 km]	0.79	0.79	0.77	0.75
0.125° [~12.50 km]	0.82	0.81	0.75	0.75
0.25° [~25.00 km]	0.81	0.83	0.77	0.76
0.5° [~50.00 km]	0.79	0.82	0.76	0.76
1.0° [~100.00 km]	0.83	0.81	0.79	0.78
2.0° [~200.00 km]	0.77	0.77	0.77	0.80

We use a single objective calibration algorithm for model calibration, however and for investigating the parameter uncertainty, we check the behavioral parameter sets with  $E_{NS}$  higher than 0.7 (an arbitrary values). These parameter sets may have very different soil parameters

combinations. Figure-3a illustrates the possible combinations of behavioral parameter sets for Case-2-4km ( $E_{NS} > 0.7$ ). As a specific example, saturated hydraulic conductivity,  $K_{sat}$ , and slope of water retention curve,  $E_{exp}$ , have very different combinations of values within the specified parameter ranges for calibration. The result indicates the two parameters that are often fixed or a priori allocated based on look up tables can exhibit significant uncertainty and non-identifiability. It is also noteworthy to mention that among the parameters,  $K_{slow}$  seems to be the most identifiable parameter while it is set to the upper limit range. There might be two explanation for this behavior: (1) this might be related to the Nivo-glacier regime of the basin of study that has strong yearly cycle due to snow accumulation and snow melt (2) and the lack of macropore water movement to the baseflow component which results in dampen input to this component and in return result in  $K_{slow}$  to be higher than expected for a baseflow reservoir (for further reading refer to Gharari et al., 2019). Overall, the results indicate that calibrating the VIC model parameters using a sum-of-squared objective function at the basin outlet does not constrain the VIC subsurface parameters. Additionally, we examine the difference between the fluxes, in this case transpiration, for all the parameter sets presented in Figure-3a. Figure 3-b illustrates differences between the yearly transpiration flux for the computational units of case-2-4km. This difference can be as high as 250 mm per year indicating the internal uncertainty of fluxes and related states in reproducing similar performance metric. This difference can be the basis of model diagnosis to understand which computational units are causing the internal uncertainty and perhaps the underlying reasons.



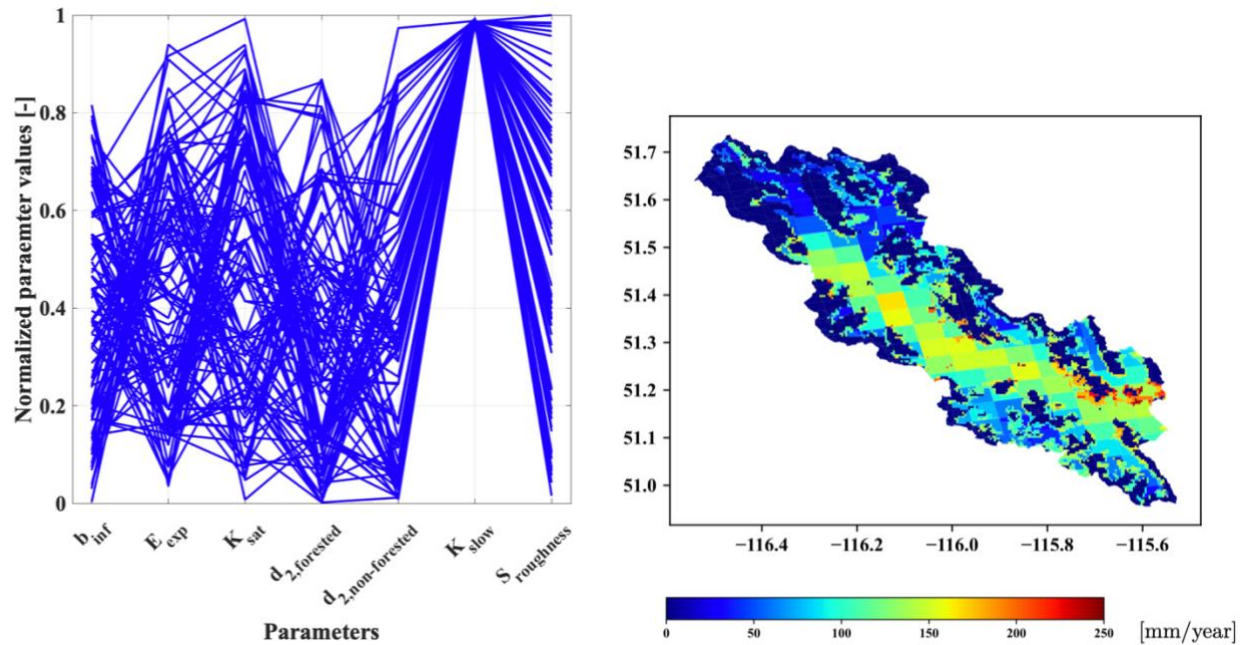
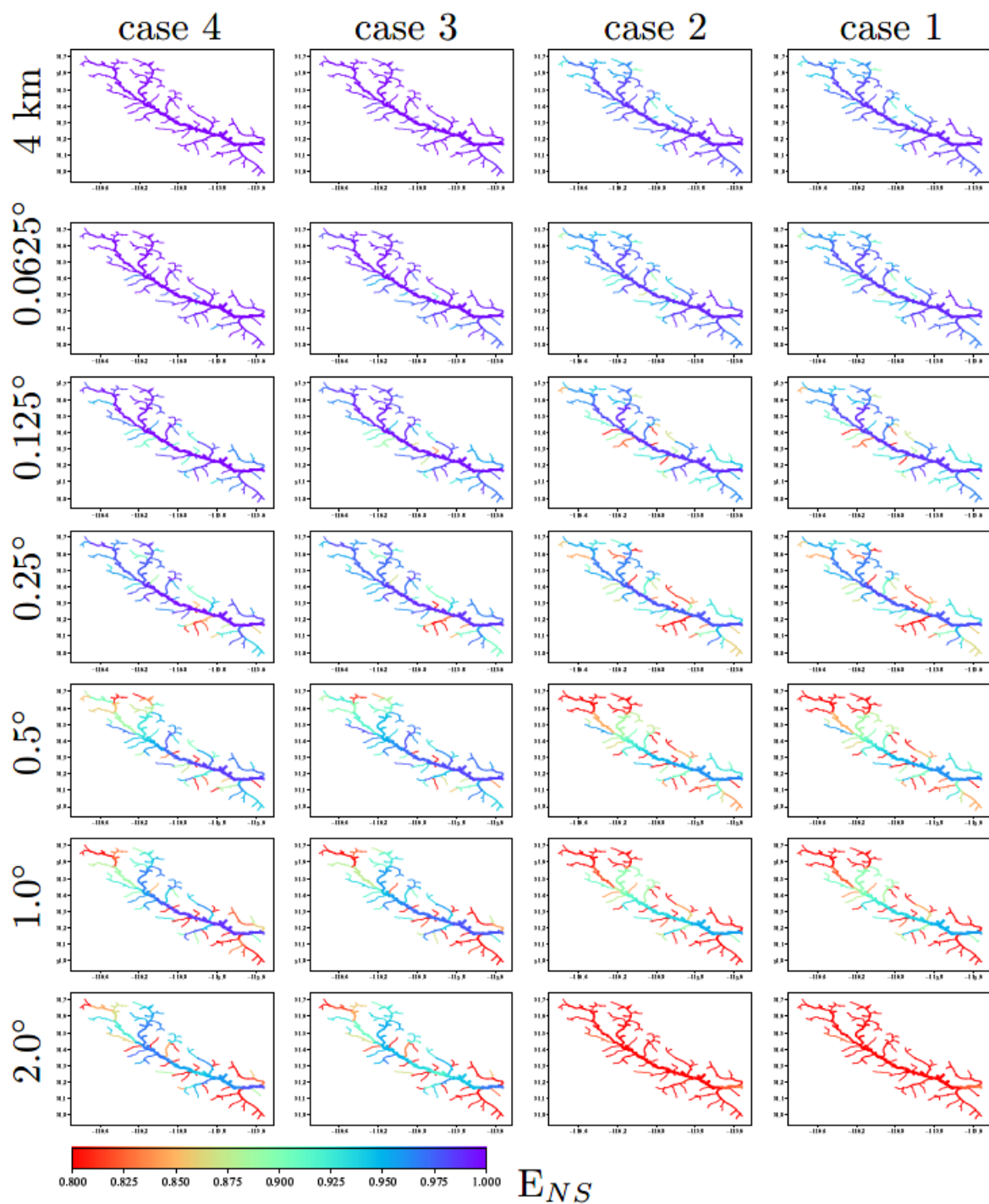


Figure-3 – (a) The normalized values for the parameters of Case-2-4km that have  $E_{NS}$ , Nash-Sutcliffe efficiency, values of higher than 0.7. (b) The difference of largest and smallest yearly simulated transpiration for parameter sets with  $E_{NS}$  above 0.7.

## 4.2 Experiment-2

The second experiment compares the performance of a parameter set from the Case-4-4km across the configurations with degraded geophysical information and aggregated spatial information. Here we choose a parameter set that has  $E_{NS}$  of above 0.7 (this can be any other parameter sets). Figure-4 shows the evaluation metric,  $E_{NS}$ , for the streamflow of every river segment across the domain in comparison with the synthetic case (Case-4-4km). From Figure-4, it is clear that the  $E_{NS}$  is less sensitive for river segments with larger upstream area (i.e. segments that are located more downstream). This result has two major interpretations (i) the parameter transferability across various configurations is dependent on the sensitivity of simulation at the scale of interest meaning that as long as good performance is achieved in the context of modeling, for example for the streamflow at the basin outlet, the parameters can be said to transferable for that scale and (ii) often inferred parameters at larger scale may not guarantee good performing parameters at the smaller

380 scales (read upstream areas) as the changed in the performance metric varies significantly across  
 381 scale for the smaller modeling elements.



382

Figure 4 – Differences of the simulated streamflow at river segments in comparison with the synthetic case, Case-4-4km, expressed in performance metric,  $E_{NS}$ .

To understand the spatial patterns of model simulations for all the configurations, we evaluate the distribution of the snow water equivalent, SWE, for the computational units on 5<sup>th</sup> of May 2004 (Figure-5). In general, the SWE follows the forcing resolution and its aggregation. Although coarser forcing resolutions results in coarser SWE simulation, the geospatial details such as elevation zones and slope and aspects result in more realistic representation of SWE as the snow layer is thinner for south facing slopes where more melt can be expected to occur, and thicker for higher elevation zones (compare SWE simulations for Case-4-2° and Case-3-2° in Figure-5) which is consistent with higher precipitation volumes and slower melt at higher elevation. Another observation from Figure-5 is the unrealistic distribution of SWE for configurations without elevation zones (Case-2 and Case-1). The lack of elevation zones results in both valley bottom and mountain tops to be forced with the same temperature. Snow is more durable in the forested areas as the result of model formulation, which are at lower elevation, while SWE is less for higher mountains, which is unrealistic. We remind the reader that the various spatial pattern of SWE across different configurations are from the simulations that results in rather similar performance metric,  $E_{NS}$ , for the streamflow at the outlet of the basin.

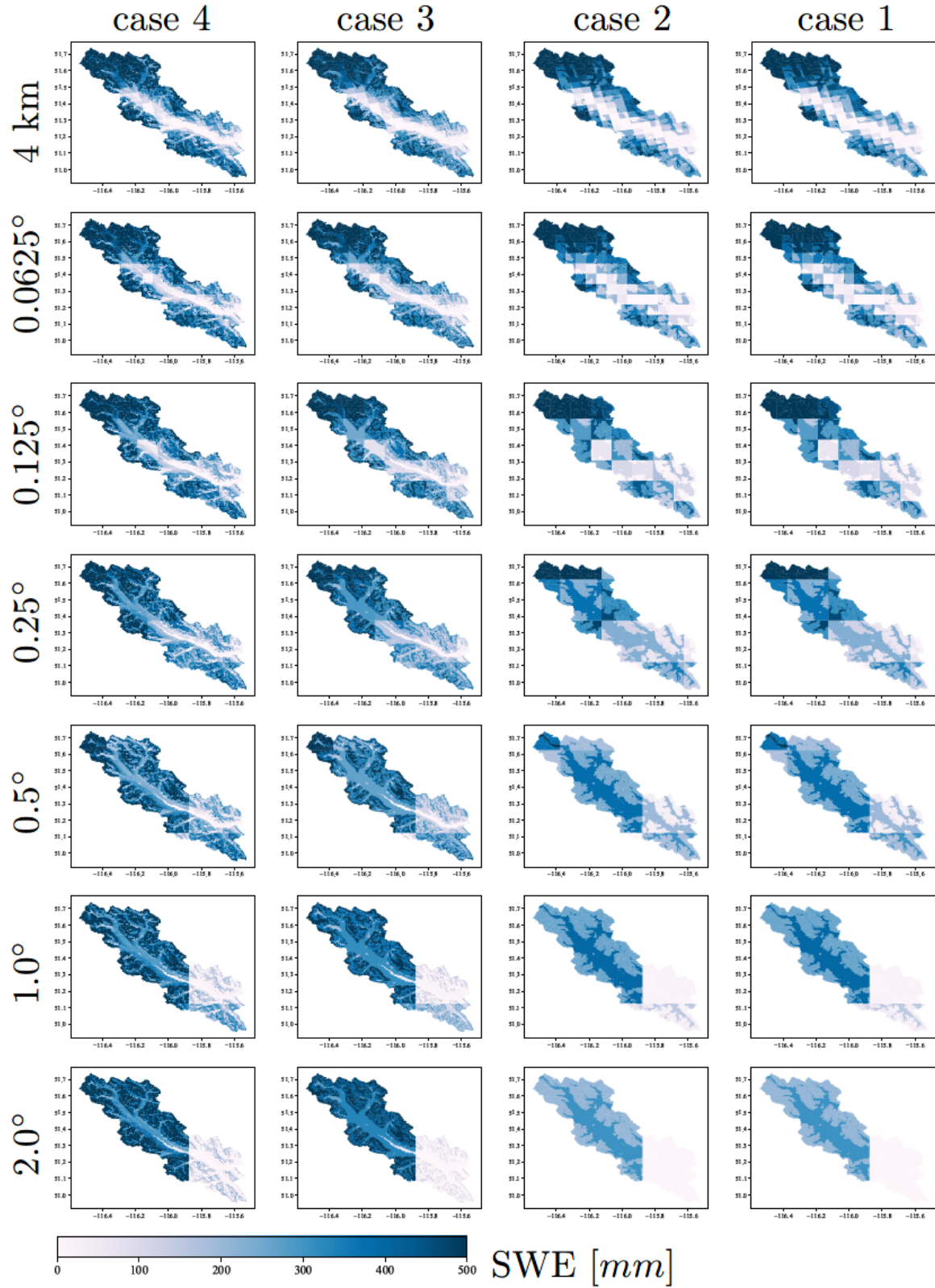


Figure 5- Comparison of the snow water equivalent for 5<sup>th</sup> of May 2004 for various configurations.

Figure-6a shows the performance of the streamflow across various configurations for the most downstream river segment (the gauged river segment which is used for parameter inference through calibration). Figure 6a illustrates that most of the configurations have similar scaled  $E_{NS}$  at the basin outlet. We compared the maximum snow water equivalent across different configurations for a computational unit located in the Bow Valley Bottom (an arbitrary location of  $-116.134^{\circ}\text{W}$  and  $51.382^{\circ}\text{E}$ ) for the year 2004 (Figure-6b). The result indicates that the SWE is higher for configurations with coarser forcing resolutions (almost triple). This is due to the reduced temperature as a result of masking warmer valley bottom by cooler and higher forcing grids over the Rockies. Such analyses can provide insights on the appropriate model configurations for different applications. Also and as an example, if model configurations of different complexity are known to show similar performance for a given parameter set, uncertainty and sensitivity analysis can be done initially on the models with fewer computational units and the results of the analysis can be applied to models with a higher number of computational units. This analysis can be repeated for different parameter sets, e.g., poorly performing parameter sets or randomly selected parameter sets, to better understand accuracy-efficiency tradeoffs of the model within its specified parameters ranges.

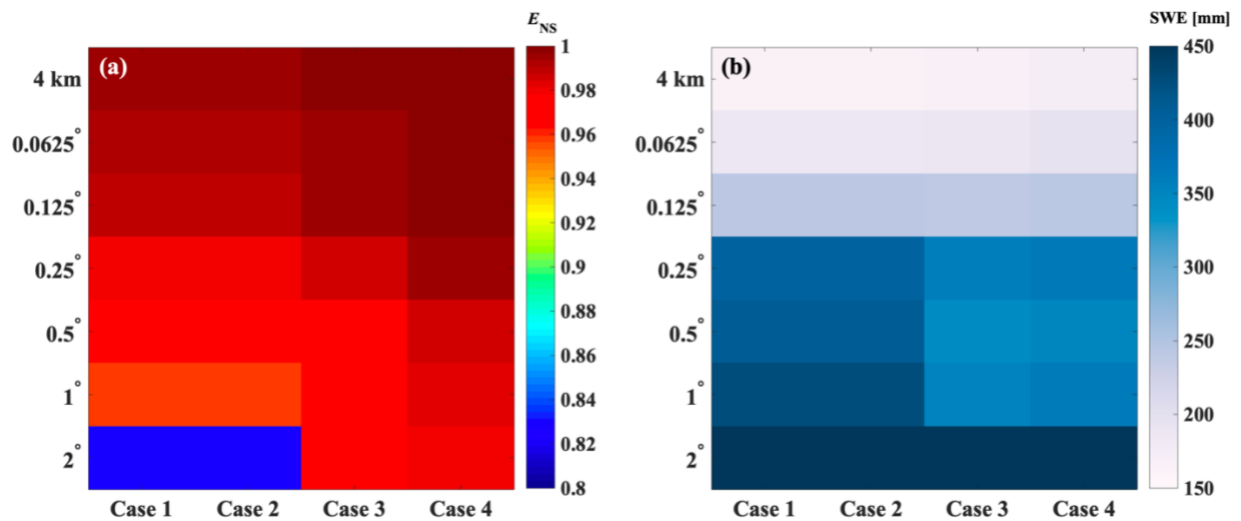


Figure -6 (a) The relative performance of model simulation across various configurations with a single parameter set. (b) Maximum of snow water equivalent for an arbitrary location of  $-116.134^{\circ}\text{W}$  and  $51.382^{\circ}\text{E}$  located in Bow Valley Bottom across various model configurations for the year 2004.

## 5 Discussion

In this study, we proposed a vector-based configuration for land models and applied this setup to the VIC model. We used a vector-based routing scheme, mizuRoute, which was forced using output from the land model (one-way coupling). Unlike the grid-based approach, there is no upscaling of land cover percentage or soil characteristics to a new grid size. This enables us to separate the effects of changes in forcing from changes in the spatial configurations. As mentioned earlier in Section 2, the vector-based configuration of land models may help avoiding unrealistic configuration of soil type, land cover or elevation zones that may happen in traditional grid-based implementation and hence increase the model fidelity. As an example, VIC configuration at grid scale assumes equal distribution of land cover over different elevation zones. Figure-7b illustrates how the traditional VIC configuration at grid-scale wrongly considers forested land cover above tree line. This issue is avoided in vector-based configuration as the set up will only include two computational unit of forested area below tree line and bare soil above the tree line (Figure 7a). The vector-based setup also provides more flexibility in comparing the model simulations across computational units (as an example, refer to Figure 5), and also comparing model simulations with point measurements, such as snow water equivalent. Moreover, the vector-based routing results in complete decoupling of the land model computational units' spatial extent from routing sub-basins. For the grid-based configuration of land models, it is often the case that in land model grid and routing grids are identical which result in further decision on upscaling of the routing direction to the land model grid scale.

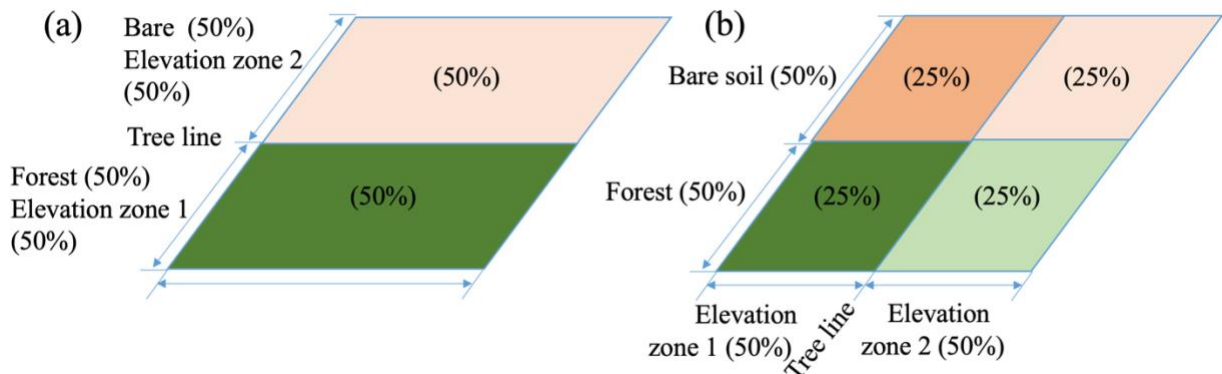


Figure-7 – (a) The realistic configuration of a natural system with land cover consist of 50% Bare soil and 50% forest within a grid located in two different elevation zones above and below the tree line which is preserved with vector-based configurations and (b) the traditional VIC configurations for the given system at the grid for the two elevation zones and 2 land cover which results in unrealistic combination of forested land cover above the tree line and bare soil below the tree line.

Our results illustrate various vector-based spatial configuration of the VIC model generates similar large-scale simulations of streamflow when the setups are calibrated by maximizing the Nash-Sutcliffe score at the basin outlet. Similarly, we have shown that often behavioral parameter sets yield similar  $E_{NS}$  and can be significantly uncertain (Figure-3a) or have significant differences for their internal behavior which may be very well masked by aggregation of the result at the grid scale or basin scale (Figure-3b and Figure-5). Generally, both parameter and states and fluxes uncertainties are not often evaluated or reported for land models (Demaria et al., 2007) or is ignored by tying parameters, linking specific hydraulic conductivity to the slope of water retention curve, for example, so that the possible combination of parameters are reduced. Moreover, the behavior of  $K_{slow}$  parameter can be revealing of the VIC model structural deficiencies which are not often explored for land models. The recession coefficient obtained from recession analysis on the observed hydrograph is approximately 0.01 1/day while the calibrated  $K_{slow}$  has much higher values of around 0.90 1/day. This can be due to damped response from the two top soil layers and lack of macropore water movement to the baseflow component. Similarly, and due to lack of macropore water movement in the VIC model, and land models in general, it is impossible to infer the  $K_{slow}$  based on recession analysis on the observed hydrograph (for further reading on this and also recession analysis refer to Gharari et al., 2019). This finding can be generalized to the 5-parameter VIC baseflow, highlighting the need to properly evaluate the often not observable but calibrated baseflow parameters for the VIC model and if it is possible to identify 5 parameters based on the recession limbs of a hydrograph.

Land models are often applied at large spatial scales. The results clearly show that the deviation of streamflow is much lower in river segments with larger upstream area (Figure 4 and 6a). It is often the case that the model parameters and associated processes are inferred through calibration



on the streamflow at the basin outlet or over a large contributing area. We argue that this may not be a valid strategy for process understanding at the smaller scale (read computational units), given the large uncertainty exhibited by the parameters. Therefore, hyper-resolution modeling efforts, Wood et al. 2011, may suffer from poor process representation and parameter identification at the scale of interest (Beven et al., 2015). What is needed instead of efficiency metrics that aggregate model behavior across both space (e.g. at the outlet of the larger catchment) and time (e.g. expressing the mismatch between observations and simulations across the entire observation period as a single number), is diagnostic evaluation of the model's process fidelity at the scale at which simulations are generated in case of available observations (e.g. Gupta et al., 2008; Clark et al., 2016).

One might argue that the spatial discretization is important for realism of model fluxes and states. Moving to significantly high number of computational units may result in computational units that are similar in their forcing and geo-spatial fabric (such as soil and land cover types). Based on the result of this study for snow water equivalent (Figure-5), we can argue that the snow patterns are fairly similar for the configurations that have elevation zones and finer resolution of forcing (case3 and 4 and forcing resolution less than 0.125 degree). It can be further explored if the model simulation at finer resolutions can be approximated by interpolating result of a model with coarser resolution ( $m(\bar{x}|\theta) \sim \overline{m(x|\theta)}$ , in which  $m$  is the model,  $x$  is forcing and  $\theta$  is the model parameter set).

The analysis on the accuracy-efficiency tradeoff presented in this study, Figure-6, can be used in model analysis such as sensitivity and uncertainty. One can assume a configuration with fewer computational units can be a surrogate for a model with more computational units, under the condition that both models are known to behave similarly for a given parameter set. The calibration can be done on the model configuration with less computational unit and the parameters can be transferred directly to the model with more computational units or can be used as an initial point for optimization algorithm to speed up the calibration process. Similarly, the sensitivity analyses can be done primarily on the model with less computational units.

In this study and following the concept hydrological similarity, we assume the parameters of computational units are identical for computational units with similar soil and land cover. The



degree of validity of hydrological similarity concepts is debatable. For example, at the catchment scale, Oudin et al. (2010) have shown that the overlap between catchments with similar physiographic attributes and catchments with similar model performance for a given parameter set is only 60%. Physiographic similarity (in our case expressed through GRUs) does thus not necessarily imply similarity of hydrologic behavior, even though this is the critical assumption underlying GRUs. The VIC parameters can be linked to many more characteristics such as slope, height above nearest drainage (HAND, Renno et al., 2008), or Topographical Wetness Index (Beven and Kirkby, 1979) as has been done by Mizukami et al. (2017) and Chaney et al. (2018). Techniques such as multiscale parameter regionalization (MPR, Samaniego et al., 2010) can be used to scale parameter values for different model configurations. However, the functions that are used to link computational units and physical attributes to model parameters remains mostly based on inference, (i.e., calibration), and the reproducibility of those relationships are not very well explored. However, applying these techniques, such as in this case that has significant parameter and process uncertainty and significance accuracy-efficiency tradeoff, should be put through rigorous tests (Merz et al., 2020, Liu et al., 2016).

A key outstanding challenge is for models to provide the right results for the right reasons (Kirchner, 2006). Thoughtful strategies to formulate parameter and process constraints based on expert knowledge can reduce the plausible range of behavioral parameter sets. In this study, we imposed a simple parameter constraint that the root zone moisture storage of forested area should be larger than the non-forested area (Table-1). Additional process constraints, if available, can be increasingly difficult to satisfy. More rigorous parameter estimation methods that satisfy the fidelity constraints based on expert knowledge are required (e.g., Gharari et al., 2014).

## **6 Conclusions**

The vector-based configuration of land models can provide modelers with more flexibility, e.g. representing the impact of various forcing resolution or geospatial data representation. The conclusions from this study can be summarized as follows:

- 1) The land model configuration with the highest number of computational units may not result in improved performance and better spatial simulation, in terms of obtained

efficiency scores, while the internal model state and fluxes can show significant uncertainty.

2) There is significant parameter and structural uncertainty associated with the land model (in this case, the VIC model). This uncertainty poses challenges for the process and parameter inference when the model is calibrated by minimizing the sum-of-squared differences between simulated and observed streamflow. Any parameter regionalization efforts should take these uncertainties into account. Our results emphasize that more attention is needed on the topic of parameter and process inference at finer modelling scales.

3) A model configuration with lower computational units, coarser resolution and less geospatial information, may reproduce model simulations with similar efficiency scores as configurations with higher computational units. Less computationally expensive configurations can be used instead for primary uncertainty and sensitivity analysis.

A key scientific challenge is hydrological scaling. i.e., how do small-scale heterogeneities shape large-scale fluxes. Addressing this challenge requires a mix of both explicit representations of spatial heterogeneity (enabled through spatial discretization of the landscape) and implicit representations of heterogeneity (enabled through sub-grid parameterizations). The contribution in this paper is to advance flexible spatial configurations for land models – our approach improves the explicit representation of spatial heterogeneities, at least compared to traditional approaches that simply drape a grid over the landscape. Much more work is required across all spatial scales to carefully evaluate how a mix of implicit and implicit representations of spatial heterogeneity can improve process representations. We encourage the community to develop tools which can enable easier and more flexible configuration of land models that can be used to explore the above-mentioned research questions.

**Acknowledgment.** This research was undertaken thanks in part to funding from the Canada First Research Excellence Fund.

**Data availability.** All the data used in this study are available publicly (refer to references).

## 7 Appendix

### 7.1 Appendix – A

This appendix reflect on the method and equations that have been used to calculate the ratio of the solar radiation on a surface with slope and aspect to a flat surface. Please note that the angles in the equations are in radian but for better communication we express angles in degree in the text.

**Declination angle:** declination angle can be calculated for each day of year and is the same for the entire Earth (Ioan Sarbu, Calin Sebarchievici, in Solar Heating and Cooling Systems, 2017):

$$\delta = 23.45 \frac{\pi}{180} \sin \left[ \frac{2\pi}{360} \frac{360}{365} (284 + d) \right] \quad (\text{A-1})$$

in which  $\delta$  is declination angle in radian and  $d$  is the number of day in a year starting from 1<sup>st</sup> of January.

**Hour angle:** hour angle is the angle expressed the solar hour. The reference of solar hour angle is solar noon (hour angle is set to zero) when the sun is passing the meridian of the observer or when the solar azimuth is 180° (north direction with azimuth of 0°). The hour angle can be calculated based on the:

$$\sin \omega = \frac{\sin \alpha - \sin \delta \sin \phi}{\cos \delta \cos \phi} \quad (\text{A-2})$$

In which  $\alpha$ ,  $\phi$  and  $\delta$  are the altitude angle, latitude of the observer and declination angle. The sunset and sunrise hour can be calculated as (when sun is at horizon and solar altitude angle is zero):

$$\cos \omega_s = -\tan \phi \tan \delta \quad (\text{A-3})$$

More caution is needed using equation A-3 for latitude above and below 66.55° north and south respectively where it can be always day or night with no sunrise or sunset during part of the year. The number of daylight hours that can be split before and after the solar noon equally can be calculated based on (assuming 15° for every 1 hour):

$$n = \frac{2\omega_s}{15} \frac{180}{\pi} \quad (\text{A-4})$$

581 And therefore, hour angle can be easily calculated for time before and after solar noon the  
 582 (relationship between the 15° equals to an hour). Hour angle is negative for the time before solar  
 583 noon and positive for the time after solar noon. Note the solar noon does not often coincide with  
 584 12 pm of the local time zone. There are relationships to find the local time of solar noon.

585 **Solar altitude angle:** Solar altitude angle is the angle of sun rays with the horizontal plane of an  
 586 observer. This angle is maximum at solar noon and 0° for subset and sunrise. The altitude angle  
 587 can be calculated based on the:

$$588 \quad \sin \alpha = \sin \delta \sin \phi + \cos \delta \cos \omega \cos \phi \quad (A-5)$$

589 For the solar noon when  $\omega$ , hour angle, is zero the question simplifies to:

$$590 \quad \sin \alpha = \sin \delta \sin \phi + \cos \delta \cos \phi = \cos(\phi - \delta) = \sin\left(\frac{\pi}{2} - \phi + \delta\right) \quad (A-6)$$

591 **Solar Azimuth:** The solar azimuth angle,  $A_{Sun}$  reflect on the angle of the sun on the sky from the  
 592 north with clockwise rule. The azimuth angle can be calculated as:

$$593 \quad \sin A_{Sun} = \frac{\sin \omega \cos \delta}{\cos \alpha} \quad (A-7)$$

594 The solar azimuth angle for the solar noon is set to be 180°.

595 The azimuth at the sunset and sunrise can be calculated:

$$596 \quad \sin A_{Sun, rise} = -\sin \omega_s \cos \delta \quad (A-8)$$

$$597 \quad \sin A_{Sun, set} = \sin \omega_s \cos \delta \quad (A-9)$$

598 **Surface Azimuth (a.k.a. aspect):** The surface azimuth angle,  $A_{Surface}$  reflect the direction of the  
 599 any tilted surface to the north direction. This azimuth is fixed for any point while the solar azimuth  
 600 changes over hours and seasons.

601 **Angle of incidence  $\theta$ :** this angle represents the angle between a sloped surface and the sun rays.  
 602 The model angle of the incidence for a slope surface  $\beta$ , and aspect of  $A_{Surface}$  over latitude of  $\phi$

can be calculated as (Kalogirou, in Solar Energy Engineering, 2009, in the reference formulation the Azimuth is from south which is corrected here for North):

$$\cos \theta = \sin \delta \sin \phi \cos \beta + \sin \delta \cos \phi \sin \beta \cos A_{Surface} + \cos \delta \cos \phi \cos \beta \cos \omega - \cos \delta \sin \phi \sin \beta \cos A_{Surface} \cos \omega - \cos \delta \sin \beta \sin A_{Surface} \sin \omega \quad (A-10)$$

For the flat surface, both  $A_{Surface}$  and  $\beta$ , is set to  $0^\circ$ , the incident angle can be calculated for the flat surface as

$$\cos \theta_{flat} = \sin \delta \sin \phi + \cos \delta \cos \phi \cos \omega \quad (A-11)$$

In case where the angle of incident is larger than  $90^\circ$  the surface shades itself.

**Correction of short-wave radiation based on slope and aspect.** In this study we correct the WRF short wave radiation based on the surface slope and aspect. We first back calculated the incoming short-wave radiation by dividing the provided short wave radiation by the cosine of the incident angle of the flat surface. Then we can calculate the solar radiation of the sloped surface multiplying this value to the cosine of the incident angle of the slope surface. Basically, this ratio is:

$$R = \frac{\cos \theta}{\cos \theta_{flat}} \quad (A-12)$$

The effect of the atmosphere is considered in the WRF product itself. However, and for incident level close to 90 degrees the ratio,  $R$ , might be very high values which result in the surface receiving unrealistically high value of radiation even higher than the solar constant, 1366 W/m<sup>2</sup>, at the top of the atmosphere. For cases with cosine values of incident angle lower than 0.05 we set the ratio to 0 to avoid this unrealistic condition.

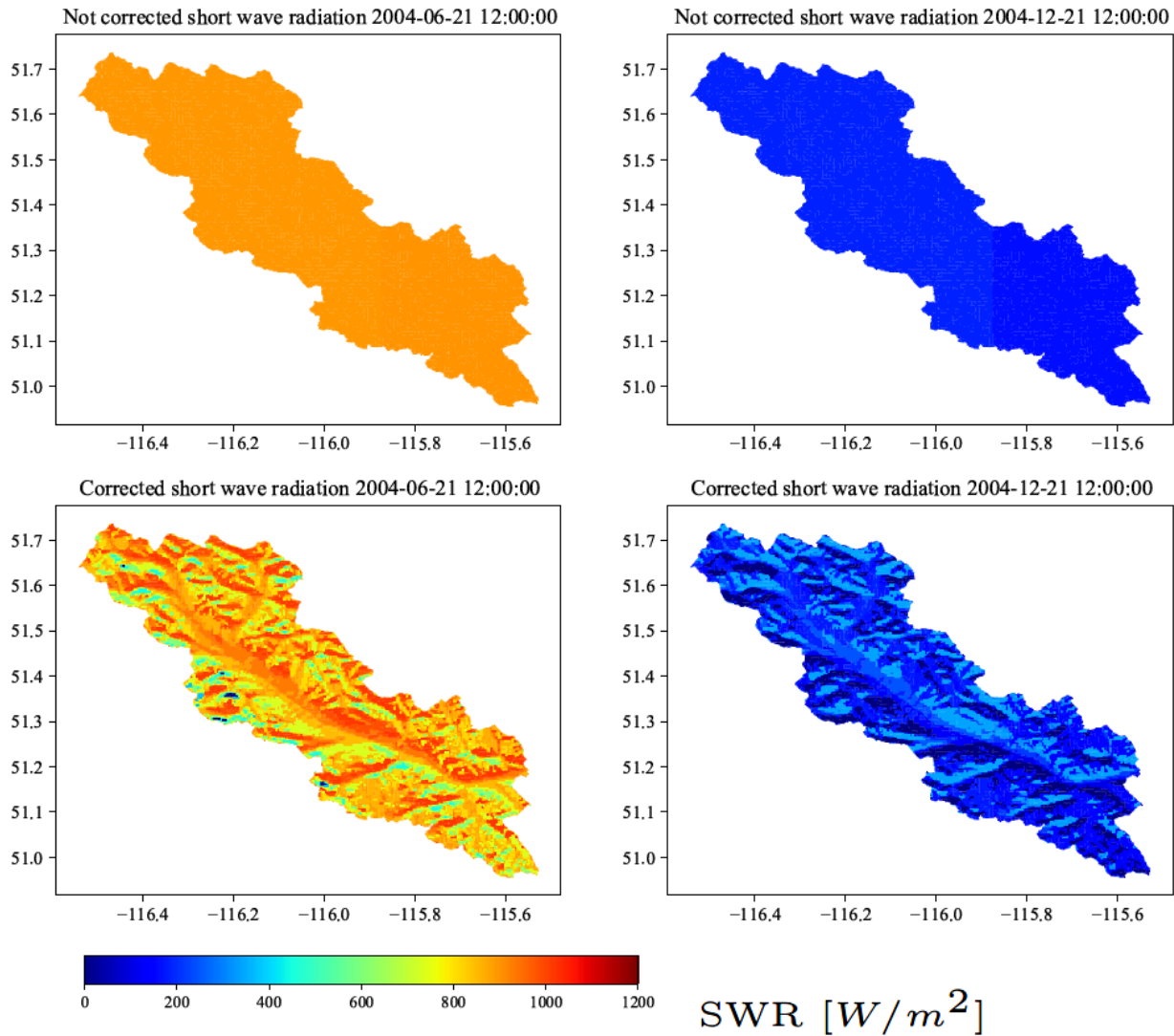


Figure A-1 Short wave radiation for (top left) not corrected for slope and aspect and (bottom left) corrected for slope and aspect for 21<sup>st</sup> June 2020 and (top right) not corrected for slope and aspect and (bottom right) corrected for slope and aspect for 21<sup>st</sup> December 2020.

## 8 References:

Annear, R.L. and Wells, S.A.: A comparison of five models for estimating clear-sky solar radiation. Water resources research, 43(10), 2007.

631 Beven, K., Cloke, H., Pappenberger, F., Lamb, R. and Hunter, N.: Hyperresolution information  
 632 and hyperresolution ignorance in modelling the hydrology of the land surface. *Science*  
 633 *China Earth Sciences*, 58(1), pp.25-35, 2015.

634 Beven, K.J. and Kirkby, M.J.: A physically based, variable contributing area model of basin  
 635 hydrology/Un modèle à base physique de zone d'appel variable de l'hydrologie du bassin  
 636 versant. *Hydrological Sciences Journal*, 24(1), pp.43-69, 1979.

637 Beven, K.J.: *Rainfall-runoff modelling: the primer*. John Wiley & Sons, 2011.

638 Blöschl, Günter, Rodger B. Grayson, and Murugesu Sivapalan: On the representative elementary  
 639 area (REA) concept and its utility for distributed rainfall-runoff modelling. *Hydrological*  
 640 *Processes* 9, no. 3-4 313-330, 1995.

641 Chaney, N.W., Van Huijgevoort, M.H., Shevliakova, E., Malyshev, S., Milly, P.C., Gauthier, P.P.  
 642 and Sulman, B.N.: Harnessing big data to rethink land heterogeneity in Earth system  
 643 models. *Hydrology and Earth System Sciences*, 22(6), pp.3311-3330, 2018.

644 Clark, M.P., Nijssen, B., Lundquist, J.D., Kavetski, D., Rupp, D.E., Woods, R.A., Freer, J.E.,  
 645 Gutmann, E.D., Wood, A.W., Brekke, L.D. and Arnold, J.R.: The structure for unifying  
 646 multiple modeling alternatives (SUMMA), Version 1.0: Technical description. NCAR  
 647 Tech. Note NCAR/TN-5141STR, 2015.

648 Clark, M.P., Slater, A.G., Rupp, D.E., Woods, R.A., Vrugt, J.A., Gupta, H.V., Wagener, T. and  
 649 Hay, L.E.: Framework for Understanding Structural Errors (FUSE): A modular framework  
 650 to diagnose differences between hydrological models. *Water Resources Research*, 44(12),  
 651 2008.

652 Clark P. M., Marc FP Bierkens, Luis Samaniego, Ross A. Woods, Remko Uijlenhoet, Katrina E.  
 653 Bennett, Valentijn Pauwels, Xitian Cai, Andrew W. Wood, and Christa D. Peters-Lidard.  
 654 "The evolution of process-based hydrologic models: historical challenges and the  
 655 collective quest for physical realism." *Hydrology and Earth System Sciences (Online)* 21,  
 656 no. LA-UR-17-27603, 2016.

Demaria, E.M., Nijssen, B. and Wagener, T.: Monte Carlo sensitivity analysis of land surface parameters using the Variable Infiltration Capacity model. *Journal of Geophysical Research: Atmospheres*, 112(D11), 2007.

Desborough, C.E.: Surface energy balance complexity in GCM land surface models. *Climate Dynamics*, 15(5), pp.389-403, 1999.

Fenicia, F., Kavetski, D. and Savenije, H.H.: Elements of a flexible approach for conceptual hydrological modeling: 1. Motivation and theoretical development. *Water Resources Research*, 47(11), 2011.

Fischer, G., F. Nachtergaele, S. Prieler, H.T. van Velthuisen, L. Verelst, D. Wiberg: Global Agro-ecological Zones Assessment for Agriculture (GAEZ 2008). IIASA, Laxenburg, Austria and FAO, Rome, Italy, 2008.

Flügel, W.A.: Delineating hydrological response units by geographical information system analyses for regional hydrological modelling using PRMS/MMS in the drainage basin of the River Bröl, Germany. *Hydrological Processes*, 9(3-4), pp.423-436, 1995.

Gharari, S., Clark, M., Mizukami, N., Wong, J.S., Pietroniro, A. and Wheeler, H., 2019. Improving the representation of subsurface water movement in land models. *Journal of Hydrometeorology*, 2019.

Haddeland, I., Lettenmaier, D.P. and Skaugen, T.: Effects of irrigation on the water and energy balances of the Colorado and Mekong river basins. *Journal of Hydrology*, 324(1-4), pp.210-223, 2006.

Haddeland, I., Matheussen, B.V. and Lettenmaier, D.P., 2002. Influence of spatial resolution on simulated streamflow in a macroscale hydrologic model. *Water Resources Research*, 38(7), pp.29-1, 2002.

Hamman, J.J., Nijssen, B., Bohn, T.J., Gergel, D.R. and Mao, Y.: The Variable Infiltration Capacity model version 5 (VIC-5): infrastructure improvements for new applications and reproducibility. *Geoscientific Model Development (Online)*, 11(8), 2018.



683 Hrachowitz, M. and Clark, M.P.: HESS Opinions: The complementary merits of competing  
684 modelling philosophies in hydrology. *Hydrology and Earth System Sciences*, 21(8),  
685 p.3953, 2017.

686 Jarvis, P.G.: The interpretation of the variations in leaf water potential and stomatal conductance  
687 found in canopies in the field. *Philosophical Transactions of the Royal Society of London.*  
688 *B, Biological Sciences*, 273(927), pp.593-610, 1976.

689 Kalogirou, S.: *Solar Energy Engineering*, edited by Soteris A. Kalogirou, 2009.

690 Kirkby, M. J. and Weyman, D. R: 'Measurements of contributing area in very small drainage basins',  
691 *Seminar Series B, No. 3. Department of Geography, University of Bristol, Bristol*, 1974.

692 Knoben, W. J. M., Freer, J. E., Peel, M. C., Fowler, K. J. A., & Woods, R. A.: A brief analysis of  
693 conceptual model structure uncertainty using 36 models and 559 catchments. *Water*  
694 *Resources Research*, 56, e2019WR025975. <https://doi.org/10.1029/2019WR025975>,  
695 2020.

696 Knudsen, J., Thomsen, A. and Refsgaard, J.C.: WATBALA Semi-Distributed, Physically Based  
697 Hydrological Modelling System. *Hydrology Research*, 17(4-5), pp.347-362, 1986.

698 Koster, Randal D., and Max J. Suarez: Modeling the land surface boundary in climate models as  
699 a composite of independent vegetation stands, *Journal of Geophysical Research:*  
700 *Atmospheres* 97, no. D3, 2697-2715, 1992.

701 Kouwen, N., Soulis, E.D., Pietroniro, A., Donald, J. and Harrington, R.A.: Grouped response units  
702 for distributed hydrologic modeling. *Journal of Water Resources Planning and*  
703 *Management*, 119(3), pp.289-305, 1993.

704 Latifovic, R., Zhu, Z., Cihlar, J., Giri, C., & Olthof, I.: Land cover mapping of North and Central  
705 America - Global Land Cover 2000. *Remote Sensing of Environment*, 89:116-127.

706 Lehner, B., Verdin, K. and Jarvis, A.: *HydroSHEDS technical documentation, version 1.0. World*  
707 *Wildlife Fund US, Washington, DC*, pp.1-27, 2006

708 Liang, X., Guo, J. and Leung, L.R.: Assessment of the effects of spatial resolutions on daily water  
709 flux simulations. *Journal of Hydrology*, 298(1-4), pp.287-310, 2004.

710 Liang, X., Lettenmaier, D.P., Wood, E.F. and Burges, S.J.: A simple hydrologically based model  
711 of land surface water and energy fluxes for general circulation models. *Journal of*  
712 *Geophysical Research: Atmospheres*, 99(D7), pp.14415-14428, 1994.

713 Liu, H., Tolson, B.A., Craig, J.R. and Shafii, M.: A priori discretization error metrics for  
714 distributed hydrologic modeling applications. *Journal of hydrology*, 543, pp.873-891,  
715 2016.

716 Manabe, Syukuro: Climate and the ocean circulation: I. The atmospheric circulation and the  
717 hydrology of the earth's surface. *Monthly Weather Review* 97, no. 11, 739-774, 1969.

718 Marsh, C.B., Pomeroy, J.W. and Spiteri, R.J.: Implications of mountain shading on calculating  
719 energy for snowmelt using unstructured triangular meshes. *Hydrological Processes*,  
720 26(12), pp.1767-1778, 2012.

721 Matott, L.S.: OSTRICH: An optimization software tool: Documentation and users guide.  
722 University at Buffalo, Buffalo, NY, 2005.

723 Maxwell, R. M., L. E. Condon, and S. J. Kollet: A high-resolution simulation of groundwater and  
724 surface water over most of the continental US with the integrated hydrologic model  
725 ParFlow v3, *Geoscientific model development* 8, no. 3, 923, 2015.

726 Melsen, L., Teuling, A., Torfs, P., Zappa, M., Mizukami, N., Clark, M. and Uijlenhoet, R.:  
727 Representation of spatial and temporal variability in large-domain hydrological models:  
728 case study for a mesoscale pre-Alpine basin. *Hydrology and Earth System Sciences*, 20(6),  
729 pp.2207-2226, 2016.

730 Merz, R., Tarasova, L. and Basso, S.,: Parameter's controls of distributed catchment models—How  
731 much information is in conventional catchment descriptors?. *Water Resources Research*,  
732 p.e2019WR026008, 2020.

733 Mizukami, N., Clark, M.P., Sampson, K., Nijssen, B., Mao, Y., McMillan, H., Viger, R.J.,  
734 Markstrom, S.L., Hay, L.E., Woods, R. and Arnold, J.R.: mizuRoute version 1: a river  
735 network routing tool for a continental domain water resources applications. *Geoscientific*  
736 *Model Development*, 9(6), pp.2223-2238, 2016.

737 Naef, F., Scherrer, S. and Weiler, M.: A process based assessment of the potential to reduce flood  
738 runoff by land use change. *Journal of hydrology*, 267(1-2), pp.74-79, 2002.

739 Newman, A.J., Clark, M.P., Winstral, A., Marks, D. and Seyfried, M.: The use of similarity  
740 concepts to represent subgrid variability in land surface models: Case study in a snowmelt-  
741 dominated watershed. *Journal of Hydrometeorology*, 15(5), pp.1717-1738, 2014.

742 Nijssen, B., O'Donnell, G.M., Hamlet, A.F. and Lettenmaier, D.P.: Hydrologic sensitivity of global  
743 rivers to climate change. *Climatic change*, 50(1-2), pp.143-175, 2001.

744 Niu, G.Y., Yang, Z.L., Dickinson, R.E. and Gulden, L.E.: A simple TOPMODEL-based runoff  
745 parameterization (SIMTOP) for use in global climate models. *Journal of Geophysical*  
746 *Research: Atmospheres*, 110(D21), 2005.

747 Niu, G.Y., Yang, Z.L., Mitchell, K.E., Chen, F., Ek, M.B., Barlage, M., Kumar, A., Manning, K.,  
748 Niyogi, D., Rosero, E. and Tewari, M.: The community Noah land surface model with  
749 multiparameterization options (Noah-MP): 1. Model description and evaluation with local-  
750 scale measurements. *Journal of Geophysical Research: Atmospheres*, 116(D12), 2011.

751 Olivera, F., Valenzuela, M., Srinivasan, R., Choi, J., Cho, H., Koka, S. and Agrawal, A.: ARCGIS-  
752 SWAT: A GEODATA MODEL AND GIS INTERFACE FOR SWAT 1. *JAWRA Journal*  
753 *of the American Water Resources Association*, 42(2), pp.295-309, 2006.

754 Oudin, L., Kay, A., Andréassian, V. and Perrin, C.: Are seemingly physically similar catchments  
755 truly hydrologically similar?. *Water Resources Research*, 46(11), 2010.

756 Park, S.J. and Van De Giesen, N.: Soil–landscape delineation to define spatial sampling domains  
757 for hillslope hydrology. *Journal of Hydrology*, 295(1-4), pp.28-46, 2004.

758 Pietroniro, A., Fortin, V., Kouwen, N., Neal, C., Turcotte, R., Davison, B., Verseghy, D., Soulis,  
 759 E.D., Caldwell, R., Evora, N. and Pellerin, P.: Development of the MESH modelling  
 760 system for hydrological ensemble forecasting of the Laurentian Great Lakes at the regional  
 761 scale. *Hydrology and Earth System Sciences Discussions*, 11(4), pp.1279-1294, 2007.

762 Pigeon, K.E. and Jiskoot, H.: Meteorological controls on snowpack formation and dynamics in the  
 763 southern Canadian Rocky Mountains. *Arctic, antarctic, and alpine research*, 40(4), pp.716-  
 764 730, 2008.

765 Pitman, A.J.: The evolution of, and revolution in, land surface schemes designed for climate  
 766 models. *International Journal of Climatology: A Journal of the Royal Meteorological*  
 767 *Society*, 23(5), pp.479-510, 2003.

768 Rasmussen, R., and C. Liu.: High Resolution WRF Simulations of the Current and Future Climate  
 769 of North America. Research Data Archive at the National Center for Atmospheric  
 770 Research, Computational and Information Systems Laboratory.  
 771 <https://doi.org/10.5065/D6V40SXP>, 2017.

772 Reggiani, P., Hassanizadeh, S.M., Sivapalan, M. and Gray, W.G.: A unifying framework for  
 773 watershed thermodynamics: constitutive relationships. *Advances in Water Resources*,  
 774 23(1), pp.15-39, 1999.

775 Rennó, C.D., Nobre, A.D., Cuartas, L.A., Soares, J.V., Hodnett, M.G., Tomasella, J. and Waterloo,  
 776 M.J.: HAND, a new terrain descriptor using SRTM-DEM: Mapping terra-firme rainforest  
 777 environments in Amazonia. *Remote Sensing of Environment*, 112(9), pp.3469-3481, 2008.

778 Samaniego, L., Kumar, R. and Attinger, S.: Multiscale parameter regionalization of a grid-based  
 779 hydrologic model at the mesoscale. *Water Resources Research*, 46(5), 2010.

780 Samaniego, L., Kumar, R., Thober, S., Rakovec, O., Zink, M., Wanders, N., Eisner, S., Müller  
 781 Schmied, H., Sutanudjaja, E., Warrach-Sagi, K. and Attinger, S.: Toward seamless  
 782 hydrologic predictions across spatial scales. *Hydrology and Earth System Sciences*, 21(9),  
 783 pp.4323-4346, 2017.

784 Sarbu, I. and Sebarchievici, C.: Thermal Energy Storage. Solar Heating and Cooling Systems,  
785 pp.99-138, 2017.

786 Savenije, H.H.G.: HESS Opinions" Topography driven conceptual modelling (FLEX-Topo)".  
787 Hydrology and Earth System Sciences, 14(12), pp.2681-2692, 2010.

788 Shafii, M., Basu, N., Craig, J.R., Schiff, S.L. and Van Cappellen, P.: A diagnostic approach to  
789 constraining flow partitioning in hydrologic models using a multiobjective optimization  
790 framework. Water Resources Research, 53(4), pp.3279-3301, 2017.

791 Shrestha, P., Sulis, M., Simmer, C. and Kollet, S.: Impacts of grid resolution on surface energy  
792 fluxes simulated with an integrated surface-groundwater flow model. Hydrology and Earth  
793 System Sciences, 19(10), pp.4317-4326, 2015.

794 Singh, R.S., Reager, J.T., Miller, N.L. and Famiglietti, J.S.: Toward hyper-resolution land-surface  
795 modeling: The effects of fine-scale topography and soil texture on CLM 4.0 simulations  
796 over the Southwestern US. Water Resources Research, 51(4), pp.2648-2667, 2015.

797 Son, K. and Sivapalan, M.: Improving model structure and reducing parameter uncertainty in  
798 conceptual water balance models through the use of auxiliary data. Water resources  
799 research, 43(1), 2007.

800 Troy, T.J., Wood, E.F. and Sheffield, J.: An efficient calibration method for continental-scale land  
801 surface modeling. Water Resources Research, 44(9), 2008.

802 Uhlenbrook, S., Roser, S. and Tilch, N.: Hydrological process representation at the meso-scale:  
803 the potential of a distributed, conceptual catchment model. Journal of Hydrology, 291(3-  
804 4), pp.278-296, 2004.

805 Vionnet, V., Fortin, V., Gaborit, E., Roy, G., Abrahamowicz, M., Gasset, N. and Pomeroy, J.W.:  
806 High-resolution hydrometeorological modelling of the June 2013 flood in southern  
807 Alberta, Canada. Hydrology and Earth System Sciences Discussions, pp.1-36, 2019.

808 Vivoni, Enrique R., Valeri Y. Ivanov, Rafael L. Bras, and Dara Entekhabi: Generation of  
809 triangulated irregular networks based on hydrological similarity, *Journal of hydrologic*  
810 *engineering* 9, no. 4, 288-302, 2004.

811 Winter, T.C.: The concept of hydrologic landscapes 1. *JAWRA Journal of the American Water*  
812 *Resources Association*, 37(2), pp.335-349, 2001.

813 Wood, E.F., Roundy, J.K., Troy, T.J., Van Beek, L.P.H., Bierkens, M.F., Blyth, E., de Roo, A.,  
814 Döll, P., Ek, M., Famiglietti, J. and Gochis, D.: Hyperresolution global land surface  
815 modeling: Meeting a grand challenge for monitoring Earth's terrestrial water. *Water*  
816 *Resources Research*, 47(5), 2011.

817 Wood, E.F., Sivapalan, M., Beven, K. and Band, L.: Effects of spatial variability and scale with  
818 implications to hydrologic modeling. *Journal of hydrology*, 102(1-4), pp.29-47, 1988.

819 Yamazaki, D., Ikeshima, D., Sosa, J., Bates, P.D., Allen, G. and Pavelsky, T.: MERIT Hydro: A  
820 high-resolution global hydrography map based on latest topography datasets. *Water*  
821 *Resources Research*, 2019.

822 Yassin, F., Razavi, S., Elshamy, M., Davison, B., Sapriza-Azuri, G. and Wheeler, H.:  
823 Representation and improved parameterization of reservoir operation in hydrological and  
824 land-surface models. *Hydrology and Earth System Sciences*, 23(9), pp.3735-3764, 2019.

825 Yoon, J.-H., Shoemaker, C. A.: Improved real-coded GA for groundwater bioremediation. *Journal*  
826 *of Computing in Civil Engineering* 15, 224-231, 2001.

827 Zhao, R.J.: The xinanjiang model. In *Proceedings of the Oxford Symposium*, 1980.